International Journal of Pressure Vessels and Piping 154 (2017) 41–57

Contents lists available at ScienceDirect

International Journal of Pressure Vessels and Piping

journal homepage: www.elsevier.com/locate/ijpvp

Residual stress measurement round robin on an electron beam welded joint between austenitic stainless steel 316L(N) and ferritic steel P91

Y. Javadi [a, *], M.C. Smith [a], K. Abburi Venkata [b], N. Naveed [c], A.N. Forsey [c], J.A. Francis [a], R.A. Ainsworth [a], C.E. Truman [b], D.J. Smith [b], F. Hosseinzadeh [c], S. Gungor [c], P.J. Bouchard [c], H.C. Dey [d], A.K. Bhaduri [d], S. Mahadevan [d]

[a] School of Mechanical, Aerospace and Civil Engineering, The University of Manchester, Manchester M13 9PL, UK
[b] Department of Mechanical Engineering, University of Bristol, Bristol BS81TR, UK
[c] Department of Engineering and Innovation, The Open University, Milton Keynes MK7 6AA, UK
[d] Indira Gandhi Centre for Atomic Research (IGCAR), Materials Development and Technology Group, Kalpakkam 603102, India

ARTICLE INFO

Article history:
Received 19 January 2017
Received in revised form
29 May 2017
Accepted 4 June 2017
Available online 8 June 2017

Keywords:
Weld residual stress (WRS)
Dissimilar metal weld (DMW)
Electron beam (EB) welding
Neutron diffraction (ND)
X-ray diffraction (XRD)
Contour method (CM)
Hole drilling (HD)

ABSTRACT

This paper is a research output of DMW-Creep project which is part of a national UK programme through the RCUK Energy programme and India's Department of Atomic Energy. The research is focussed on understanding the characteristics of welded joints between austenitic stainless steel and ferritic steel that are widely used in many nuclear power generating plants and petrochemical industries as well as conventional coal and gas-fired power systems. The members of the DMW-Creep project have undertaken parallel round robin activities measuring the residual stresses generated by a dissimilar metal weld (DMW) between AISI 316L(N) austenitic stainless steel and P91 ferritic-martensitic steel. Electron beam (EB) welding was employed to produce a single bead weld on a plate specimen and an additional smoothing pass (known cosmetic pass) was then introduced using a defocused beam. The welding residual stresses have been measured by five experimental methods including (I) neutron diffraction (ND), (II) X-Ray diffraction (XRD), (III) contour method (CM), (IV) incremental deep hole drilling (iDHD) and (V) incremental centre hole drilling (iCHD). The round robin measurements of weld residual stresses are compared in order to characterise surface and sub-surface residual stresses comprehensively.

1. Introduction

The DMW-Creep project is part of an international scientific collaboration between the UK research councils and India's Department of Atomic Energy. Four universities, Manchester, Bristol, Oxford, and the Open University, are working with the Indira Gandhi Centre for Atomic Research (IGCAR). DMW-creep is focussed on understanding the characteristics of electron beam (EB) welded joints between austenitic stainless steel (AISI Type 316LN) and ferritic-martensitic steel (P91). This type of weld, known as dissimilar metal weld (DMW), is extensively used in nuclear power generating plants. For instance, IGCAR is responsible for the design of the Prototype Fast Breeder Reactor (PFBR) in which the steam generator (made of P91) is required to be joined with the intermediate heat exchanger (made of AISI 316LN) [1,2].

Welding leads to the development of significant residual stresses. These are the stresses remaining inside the material in the absence of any external loads or thermal gradients. Dissimilar metal welds offer several complications not found in similar metal welds. For instance, the AISI 316L(N) stainless steel has a thermal conductivity of one-half of P91 while the coefficient of thermal expansion is 45% greater than P91. These mismatches in material properties result in differing stress profiles on either side of the weld. AISI 316L(N) and P91 offer the further complication that P91, which is normally martensitic, undergoes solid-state phase transformation (SSPT) in the heat affected zone while AISI 316, which is austenitic, does not. It is important to quantify the levels of residual stress in critical components such as those operating at high temperatures in nuclear plants, since they can significantly impact in-service performance.

The measurement of residual stresses can be achieved through non-destructive methods (e.g., ultrasonic techniques [3], X-Ray

* Corresponding author.
E-mail address: yashar.javadi@manchester.ac.uk (Y. Javadi).

http://dx.doi.org/10.1016/j.ijpvp.2017.06.002

diffraction [4,5] and Neutron diffraction [6]), semi-destructive methods (e.g., hole-drilling [7]) or destructive methods (e.g., the contour method [8]). X-Ray diffraction (XRD) is a surface measurement method providing stresses over a depth of a few tens of microns [9]. In steels, ultrasonic methods and neutron diffraction (ND) have penetration depths limited to 6 mm ([10]) and 20–30 mm ([6]), respectively. The incremental centre hole-drilling (iCHD) technique employs a strain gauge rosette to measure the strains relaxed by incremental drilling of a small hole. Since the hole-drilling method is standardised by ASTM E837, it is often used as a verification tool for other stress measurement methods [11–15]. The incremental deep hole drilling (iDHD) is conducted by drilling a reference hole through the specimen and precisely measuring the hole diameter before and after stress release, achieved by trepanning coaxially to the reference hole using electro-discharge machining (EDM) [16]. The contour method (CM) is a destructive technique that requires the sample of interest to be cut perpendicular to the stress direction of interest using electro-discharge machining (EDM) which does not impart contact stress onto the cut surface. The topography on the two cut faces is then measured, averaged and applied (in reverse) as a deformation to a flat surface of a finite element model of half the original sample [8]. The deformation is assumed to proceed entirely elastically, and the stress engendered is, by a modification of Bueckner's principle, equivalent to the stress released when the part was sectioned [17]. A 2D map of the stresses acting in the direction perpendicular to the cut surface is produced over the whole of the cut surface.

The characterisation of welding residual stress (WRS) by measurements is accompanied by a range of uncertainties [18] caused by random and systematic errors in the stress measurement techniques. Hence, a reliable characterisation of WRS necessitates a well-designed methodology using diverse independent measurement techniques [19].

Kerr et al. [20] conducted a combination of neutron diffraction, contour method, and hole drilling residual stress measurements on a DMW plate specimen, fabricated from a 304L stainless steel plate and Nickel Alloy 82 weld, and compared the experimental measurements to a finite element weld modelling results. Although the neutron and contour method stress measurement results did not agree very well, it was recommended to use at least two techniques that have different assumptions to increase the accuracy of the experimental results. However, in specimens other than fusion welds, there is usually an acceptable agreement between the contour method measurements with the neutron diffraction or synchrotron diffraction measurements [21–24]. This agreement had been sometimes quite good [25,26] but often not convincing [27,28] in the welded components.

In this study, a residual stress measurement round robin has been conducted by using all the aforementioned methods (i.e., XRD, ND, iCHD, iDHD and CM) to measure the weld residual stress (WRS) in the dissimilar metal welded specimen shown in Fig. 1.

2. Conduct of round robin residual stress measurement

2.1. DMW specimen manufacture

The DMW specimen was manufactured using autogenous electron beam welding to join plates of austenitic stainless steel (AISI 316LN) and ferritic-martensitic steel (P91), using a penetration pass followed by a second smoothing pass (cosmetic pass) to fill the surface slot left after completion of the first pass. As shown in Fig. 1, the specimen had dimensions 250 × 156 × 11.2 mm and the materials had the chemical compositions and material properties shown in Table 1 and Table 2, respectively. The plates were restrained during welding by a clamping system shown in Fig. 2. A tungsten inert gas (TIG) welding machine was then employed to perform a small number of tack welds in order to ensure that the weld plates were correctly aligned throughout the EB welding process. However, due to a concern about cracking of the tack welds caused by the high energy EB beam, along with high-speed welding process, the tack welds were recognised not to be sufficient for holding both the plates in position. Hence, the joining edges were also melted up to a depth of 1.5 mm in order to hold the plate in the right position and withstand the high beam force and thermal stress. In order to reduce mismatch caused by thermal conductivity difference between P91 and AISI 316L(N), the P91 plate was first preheated. The defocused beam of very low power was passed on the P91 plate adjacent to the weld line in order to preheat the plate. Although there was no provision to measure the preheating temperature, as the welding was carried out in a vacuum chamber, the beam parameters were set to reach a preheating temperature of 150–200 °C. The EB weld was then started comprising one penetration pass in keyhole mode followed by a lower power smoothing pass (known as a cosmetic pass) as shown in Fig. 1. The cosmetic pass is necessary as the main pass leaves some surface defects, which require removal by machining or repair by re-melting through a subsequent weld pass. A defocused beam is employed to complete the cosmetic pass with different welding parameters from those used for the main pass, as shown in Table 3. The penetration depth and fusion zone dimensions have been subsequently measured by metallography as shown in Fig. 3.

2.2. WRS measurement by X-Ray diffraction

The X-ray diffraction (XRD) method is able to measure surface residual stresses non-destructively [4]. Fitzpatrick et al. [5] published a good practice guide for determination of residual stress by the XRD. Laboratory-based or portable equipment, can measure residual stresses to depths of up to 30 μm [4]. The application of XRD on the DMW specimen was on a surface line perpendicular to the weld and at the centre of the weld length, extending across weld, HAZ and both parent materials for a total distance of 80 mm, as shown in Fig. 1. Only longitudinal stresses were measured. These measurements were performed at the Indira Gandhi Centre for Atomic Research (IGCAR).

2.3. WRS measurement by the neutron diffraction

The neutron diffraction (ND) method exploits Bragg's Law to detect any changes in atomic lattice spacing caused by stresses in the component, using the lattice spacing as a strain gauge. ISO/TS 21432:2005 has provided the standard test method for determining residual stresses in polycrystalline materials by the ND [31]. The method requires lattice-spacing measurements in a stress-free material sample to obtain the stress-free lattice parameter (known as a d_0 sample) to calculate absolute stress values. Neutron diffraction may be used to measure bulk stresses, at depths of tens of mm, rather than a few tens of μm [32]. Neutron diffraction measurements were made on the pulsed diffractometer ENGIN-X, at the ISIS facility, Rutherford Appleton Laboratory in Oxford. The specimen was first machined to remove the reference samples (for stress-free lattice parameter measurement) and then all the reference samples as well as the specimen were measured at the same time.

ENGIN-X employs time-of-flight scattering and produces diffraction patterns over a range of grain families oriented along various crystallographic planes which permit the residual stress/strain state in multiple phases to be measured [1]. As shown in Fig. 1, the residual stresses were characterised along a line transverse to the weld at the centre of the plate and at a depth of 5.5 mm

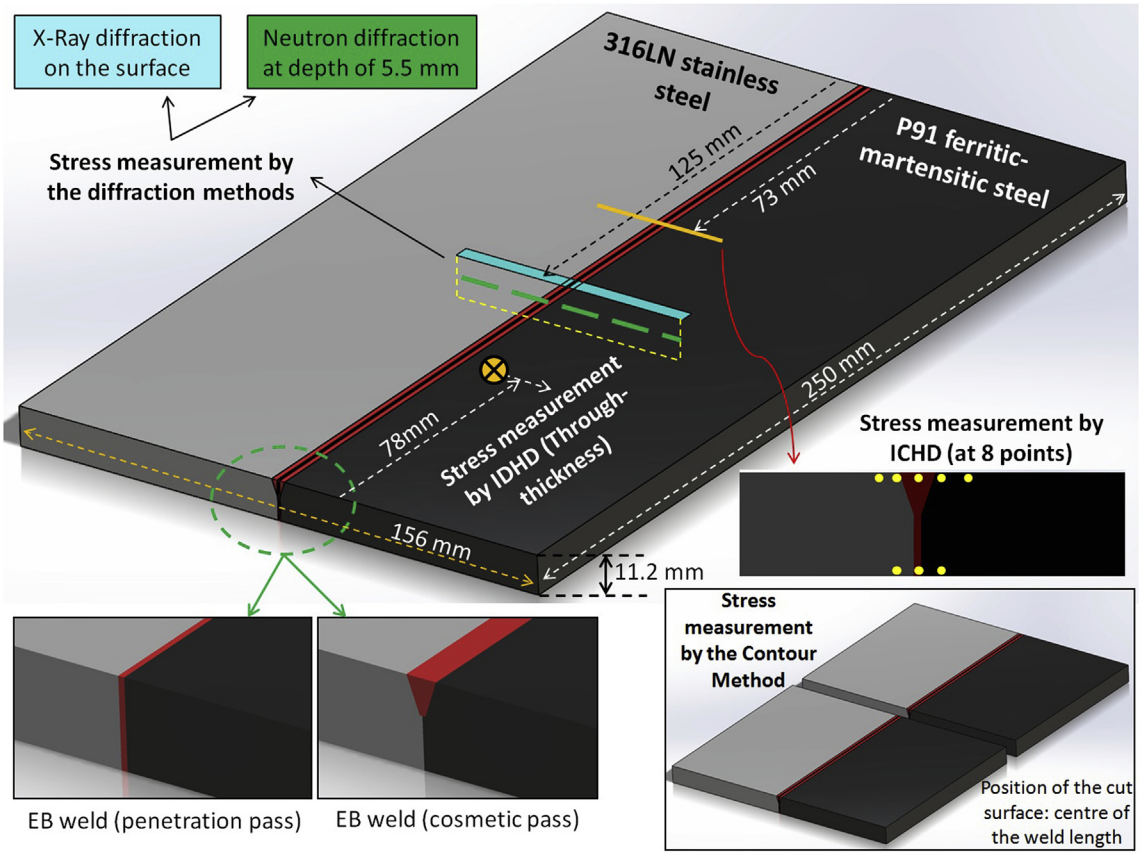

Fig. 1. WRS measurement round robin on a DMW produced by EB welding process.

Table 1
Chemical composition of P91 and AISI 316L(N) [1].

	C, %	Mn, %	Cr, %	Ni, %	Mo, %	Nb, %	Cu, %	N, %	Fe, %
P91	0.11	0.39	8.82	0.21	0.82	0.07	0.17	0.0464	Balance
316L(N)	0.03	1.72	17.5	11.9	2.58	0.005	0.195	0.087	Balance

from the top surface. This measurement depth was chosen to ensure that the measured points in weld metal were in the first pass rather than the cosmetic pass, see Fig. 3. The measurement intervals in the weld and the HAZ region were evenly spaced but smaller than those selected for the parent material as shown in Fig. 4a. In order to measure the stress free lattice parameter, specimens were removed separately from the weld, HAZ and parent material as shown in Fig. 4b and c. The gauge volume was $1 \times 1 \times 1$ mm and the incoming beam size was 1×1 mm for the longitudinal direction.

The ND measurements were carried out in three orthogonal directions. The longitudinal residual stress is parallel to the weld length, the transverse residual stress is perpendicular to the weld length and the normal direction is through the thickness of the specimen. These were assumed to be principal stress directions.

As the neutrons originated from a pulsed source, the reflections were obtained from different crystallographic planes and Pawley-Rietveld refinement was used to fit the diffraction peaks [1]. Direction and position dependent lattice constant measurement on the stress-free samples were used to calculate the strains in the respective stress directions. The strains and stresses were calculated using [33,34]:

$$\varepsilon_{xx} = \frac{a_x - a_{0x}}{a_{0x}} \tag{1}$$

$$\sigma_{ij} = \frac{E}{(1+\nu)}\left[\varepsilon_{xx} + \frac{\nu}{(1-2\nu)}\left(\varepsilon_{xx} + \varepsilon_{yy} + \varepsilon_{zz}\right)\right] \tag{2}$$

In Eqs. (1) and (2), ε_{xx} is the strain along the direction of x; a_x and a_{0x} are representing the stress free lattice parameter in the direction of x; E is Young's modulus and ν is the Poisson's ratio. The values of Young's modulus were assumed to be 210 GPa for P91 steel and 195.6 GPa for AISI 316L(N) stainless steel. The Poisson's ratio was assumed to be 0.3 for BCC material and 0.29 for FCC material. These values correspond to the recommendations from Kroner's models for the macroscopic elastic bulk properties in poly-

Table 2
Material properties of P91 and AISI 316L [29,30].

	Thermal expansion coefficient $\times 10^{6}$°C^{-1}	Young's Modulus (GPa)	Yield Stress (MPa)		Poisson's ratio
			Parent material	Weld	
P91	10.4	210	489	550	0.3
316L(N)	14.56	195.6	210	250	0.29

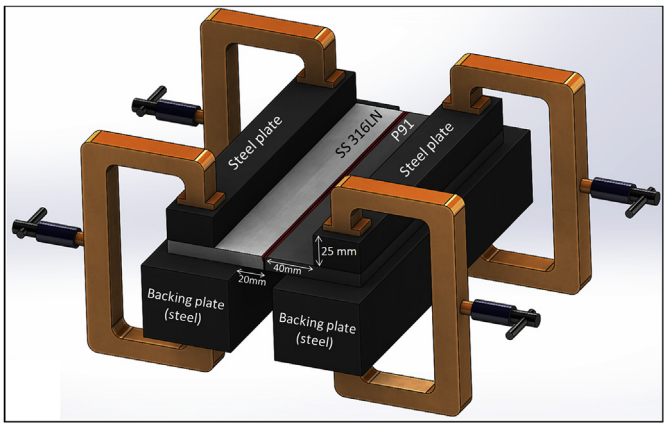

Fig. 2. Clamp configuration in EB welding of the DMW specimen.

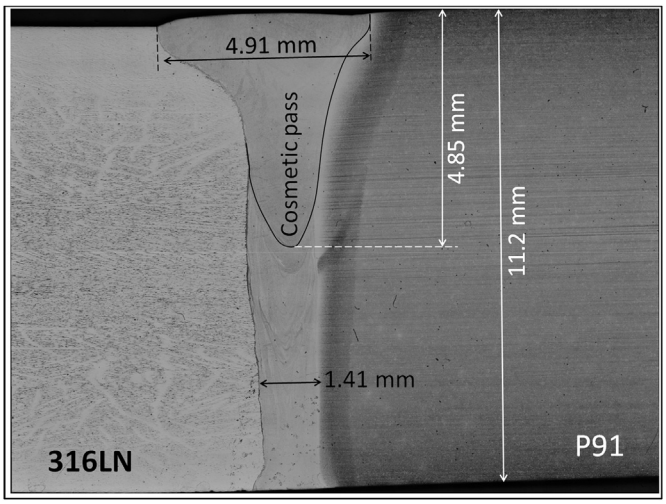

Fig. 3. Penetration depth and fusion zone dimensions.

crystals for the BCC and FCC phases [34].

2.4. WRS measurement by hole drilling methods

The hole drilling methods used in this study were divided into shallow and deep measurements through the plate thickness, employing the incremental centre hole drilling (iCHD) and deep hole drilling (DHD) techniques, respectively. The iCHD technique was employed for near-surface residual stress measurements at eight points as shown in Fig. 1. The measurements were carried out by VEQTER Ltd and based on ASTM-E837-13a measurement standard [35].

The deep hole drilling (DHD) method, developed at the University of Bristol since the early 1990s [16], is based on the analytical solution for the deformation of a hole in an infinite plate under biaxial loading. The experimental process includes four steps. In Step 1, a small reference hole is drilled through the specimen. In Step 2, the diameter of the hole is accurately measured at multiple angular positions and depths. In Step 3, a column of material is coaxially trepanned using electro-discharge machining (EDM). Finally, Step 4 is a repeat of the process already carried out in Step 2 and at the same angular positions and depths [36]. The distortion of the reference hole diameter in the plane normal to the reference hole axis is used to determine the in-plane residual stress field.

If high magnitude residual stresses are present, then the incremental DHD (iDHD) technique is employed to account for plasticity during the stress relieving process (i.e. Step 3) [32]. During the iDHD process, Step 3 is carried out incrementally along with the diameter measurements (i.e. Step 4) at each of the increments. Steps 3 and 4 are then replicated until the completion of the EDM cutting process.

Both the DHD and iDHD methods were applied on the DMW specimen in one hole located at 78 mm distance from the edge, as shown in Fig. 1, and in the P91 side (at 4.6 mm distance from the weld centerline). The gun-drilled hole, Step 1, had a diameter of 1.5 mm while the trepanned core, Step 3, had an external diameter of 4 mm. The experimental lab and measurement activities were provided by the University of Bristol [16].

2.5. WRS measurement by the contour method

The contour method, which falls into the category of destructive stress measurement methods, is a conceptually simple and data-rich means of determining a two-dimensional cross-section of a single component of the residual stress field in a body [37]. A good practice guideline for the contour method has been published by Hosseinzadeh et al. [38]. It is a three-step process, as shown in Fig. 5, whereby the component of interest is first sectioned to relieve stresses acting normal to the cut surface. The deformations of the two cut surfaces are then measured and averaged. This averaged surface is then used as the input boundary conditions for a finite element model in which the deformed surface is forced back to being flat, and the forces required to do so are calculated.

When sectioning the component, the normal and shear stresses on the cut plane are relieved, and two traction free surfaces are created. The requirements for a representative, and hence successful, finite element analysis are that all relaxations on the cut surface should take place within the elastic regime that the cutting process itself should not introduce any stresses which will affect the deformation of the cut surface, and that the cut width, when measured in the original undeformed part, should be constant along its whole length. This last requirement or assumption is usually simplified to say that the cut surface should be perfectly planar in space and therefore all deviations from planarity can be attributed to deformation from the relaxation of the stresses. In light of these requirements, Wire Electro-Discharge Machining (EDM) is commonly used for the contour method, which is a non-contact cutting technique that does not impart any stress to the material during cutting. EDM cutting the specimens is the most crucial step of the contour method process.

If the cutting process is ideal (or as close to ideal as possible) then two traction free surfaces will be created where the normal stress and the shear stresses on that surface are zero. In step 3, by measuring the deformations due to surface relaxation, it is then possible to determine the stresses that were present by considering

Table 3
Welding parameters.

	Beam current	Gun voltage	Welding speed	Penetration depth	Weld width
1st Pass (full penetration weld with focused beam)	48 mA	120 kV	500 mm/min	11.2 mm	1.4 mm
Cosmetic pass (defocused beam)	26 mA	100 kV	500 mm/min	4.85 mm	4.91 mm

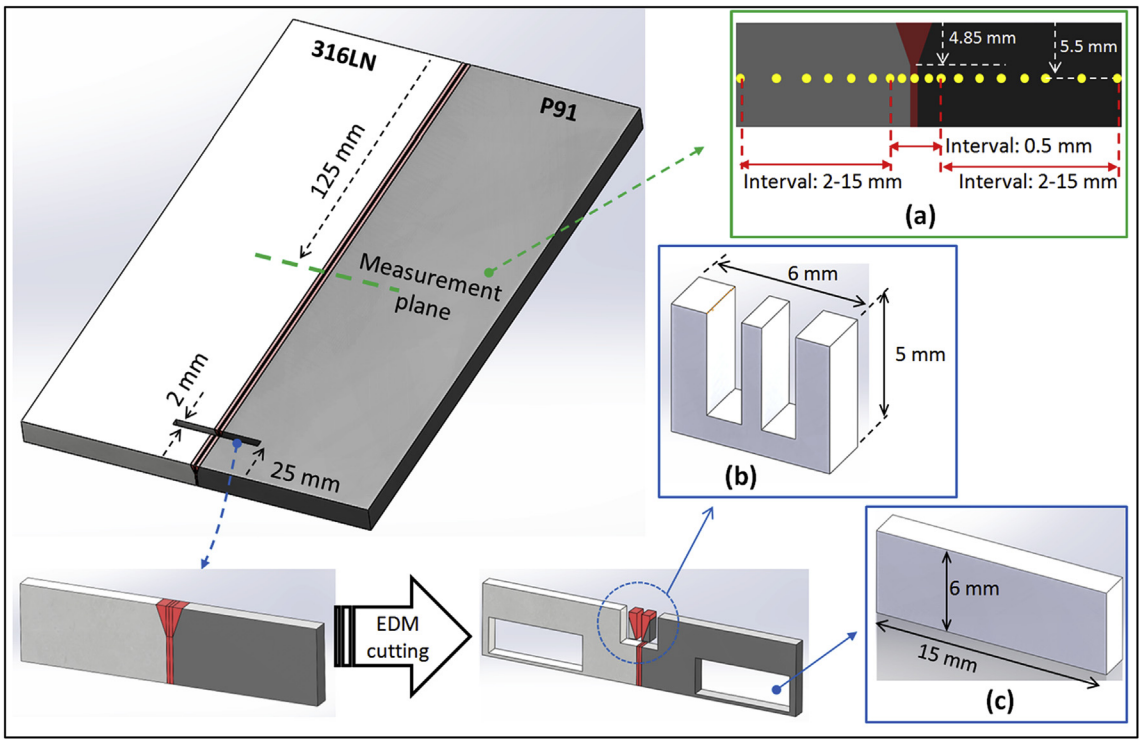

Fig. 4. Measurement intervals used during ND at depth of 5.5 mm (a) as well as the stress-free specimens extracted from the weld/HAZ (b) and from the parent material (c).

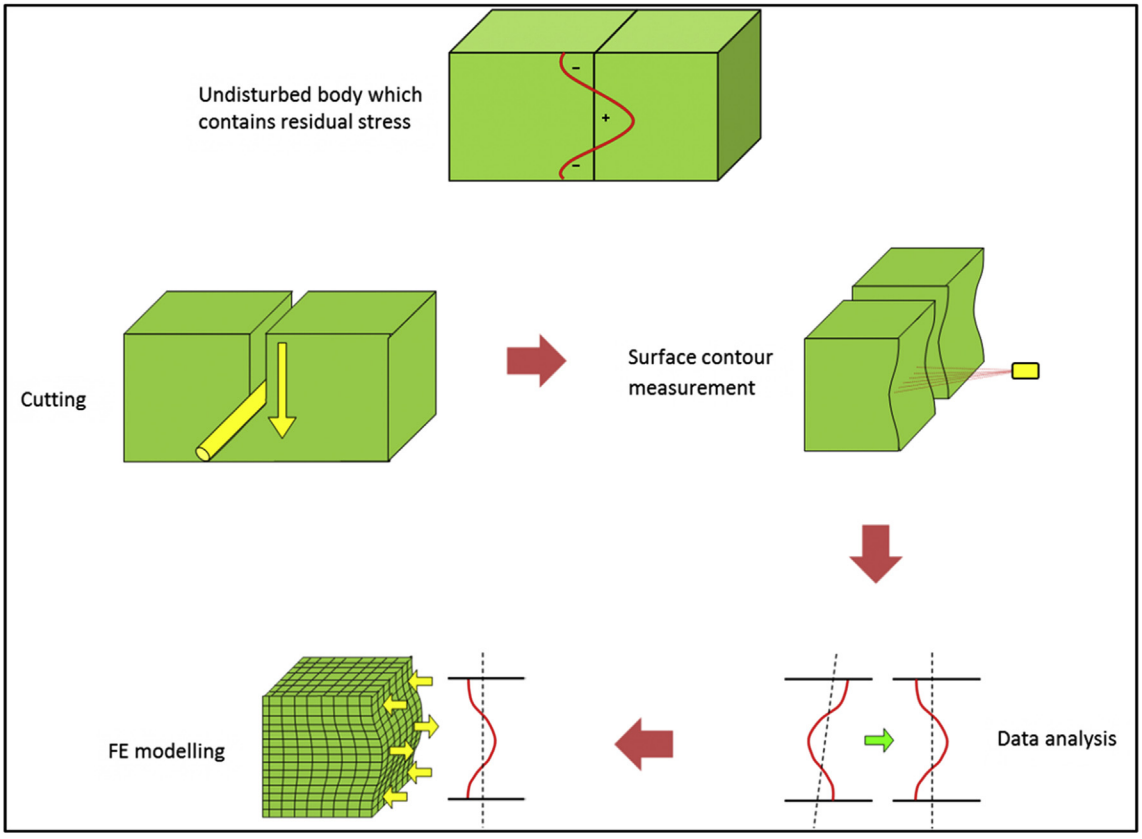

Fig. 5. Stress measurement by the contour method.

equivalent surface tractions on the cut plane. The deformations due to the normal stress will be symmetric on both cut surfaces; the shear stresses, which affect the surface through the Poisson effect, produce antisymmetric deformations. During the contour method, both cut surfaces are measured and their deviation from a planar surface is averaged to produce a single surface for analysis [8]. Averaging of the two surfaces cancels out the antisymmetric strains due to the shear stresses, and the antisymmetric noise in the data from the cutting process. Thus the contour method relies on the precision and accuracy of the measurement of deviation from planarity of the cut surface.

The contour method measurement on the DMW specimen was performed by the Open University. A single EDM wire cut was carried out using 50 μm diameter wire and 3 mm entry and exit pilot holes placed 20 mm from the sample edge. This results in a self-constrained embedded cut [39], which reduces the likelihood of plastic deformation and bulging errors affecting the sample during the cut. The 50 μm wire produces a cut with very low roughness, which helps to reduce uncertainty in the surface measurement: the result of which is shown in Fig. 6. The contour surface measurement was made using a Mitutoyo Crysta plus 547 CMM with a 1 mm diameter Renishaw PH10 M touch trigger probe. A measurement pitch of 0.125 mm was used to enable the expected short length scale variation at the weld line to be resolved. The surface measurement was smoothed using bicubic splines and an optimised knot spacing of 0.5 mm [40], which produced a minimum average stress uncertainty of 17 MPa. These data were then used as surface boundary conditions for a linear elastic finite element analysis using ABAQUS. The cut surface was meshed with 0.25 mm × 0.25 mm linear hexahedral elements, with material properties for the P91 taken as $E = 210$ GPa, $\nu = 0.3$ and for the AISI 316L(N), $E = 195.6$ GPa and $\nu = 0.29$. This model was then used to perform an elastic FE analysis to determine the residual stress distribution.

Cutting artefacts are visible as vertical lines perpendicular to the cutting direction in the cut surfaces in Fig. 6. These features are present in both surfaces and lead to inaccurate residual stress measurements in these regions. As the EDM cut is influenced by any change in the material properties, achieving a smooth cut without artefacts is often not practical for a dissimilar metal specimen. The artefacts reported during the cutting process of the DMW specimen are marked in Fig. 6.

3. Results and discussion

3.1. Bulk stress measurement

3.1.1. Results achieved by the contour method

The longitudinal residual stress distribution measured using the contour method is shown in Fig. 7. The dark blue regions in both penetration and cosmetic passes suggest compressive stresses in the weld bead. This is consistent with the effects of low-temperature solid-state phase transformation (SSPT) on the stress state in the high energy EB welds [41,42]. The weld metal, containing a composition intermediate between AISI 316L(N) and P91, have been subjected to a martensitic transformation at low temperature after solidification. The resulting volumetric expansion from face-centered cubic (FCC) to body-centered cubic (BCC) structure generates the compressive stresses observed in the weld bead. There are two dark blue regions at top of the weld as well as large red and orange regions at both sides of the cosmetic pass in the AISI 316L(N) and P91 parent material. These indicate that the stresses within and adjacent to the cosmetic pass are more tensile in the parent material, and more compressive in the weld bead, in comparison with the stresses within and adjacent to the penetration pass. In order to compare the results with those obtained from the other stress measurement methods, the contour method results at a depth of 1 mm and 5.5 mm from the top surface as well as at 1 mm from the bottom surface are plotted in Fig. 8. Fig. 8 plots stresses at the depth chosen for neutron diffraction measurements, 5.5 mm from the top surface. There are high magnitude compressive stresses in the weld bead (−368 MPa) and stresses rise sharply on both sides of the weld to reach 352 MPa and 459 MPa on P91 and AISI 316L(N) sides, respectively. As previously shown in Fig. 6, there are artefacts in the measured stresses on both the P91 and AISI 316L(N) sides, with artificial stresses at around −35 mm, −7 mm, 5 mm and 18 mm.

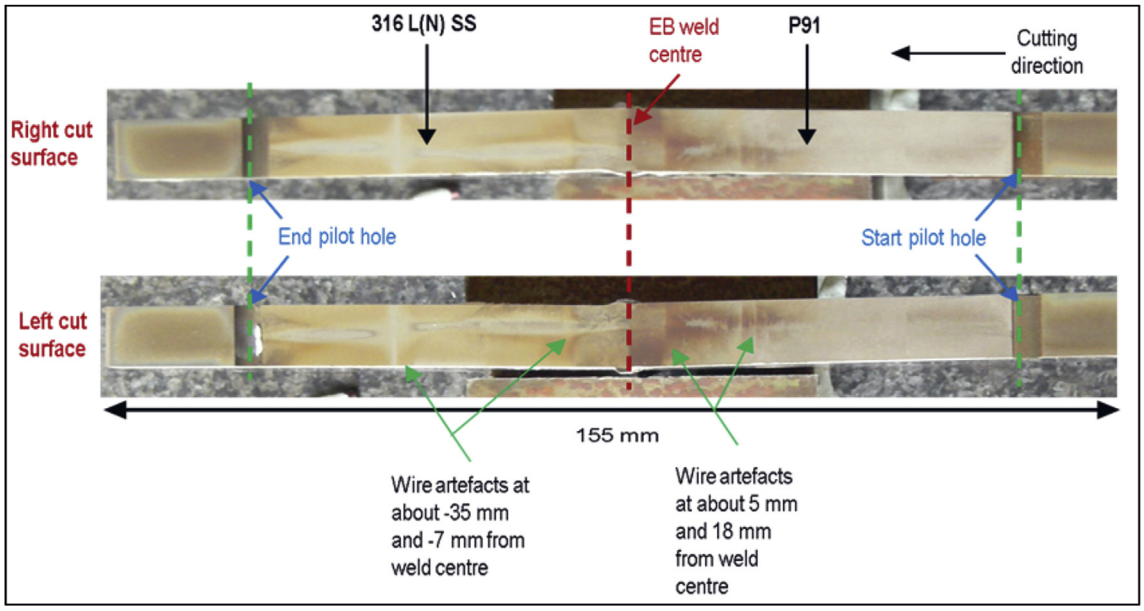

Fig. 6. Image of contour cut surfaces with cut details overlaid.

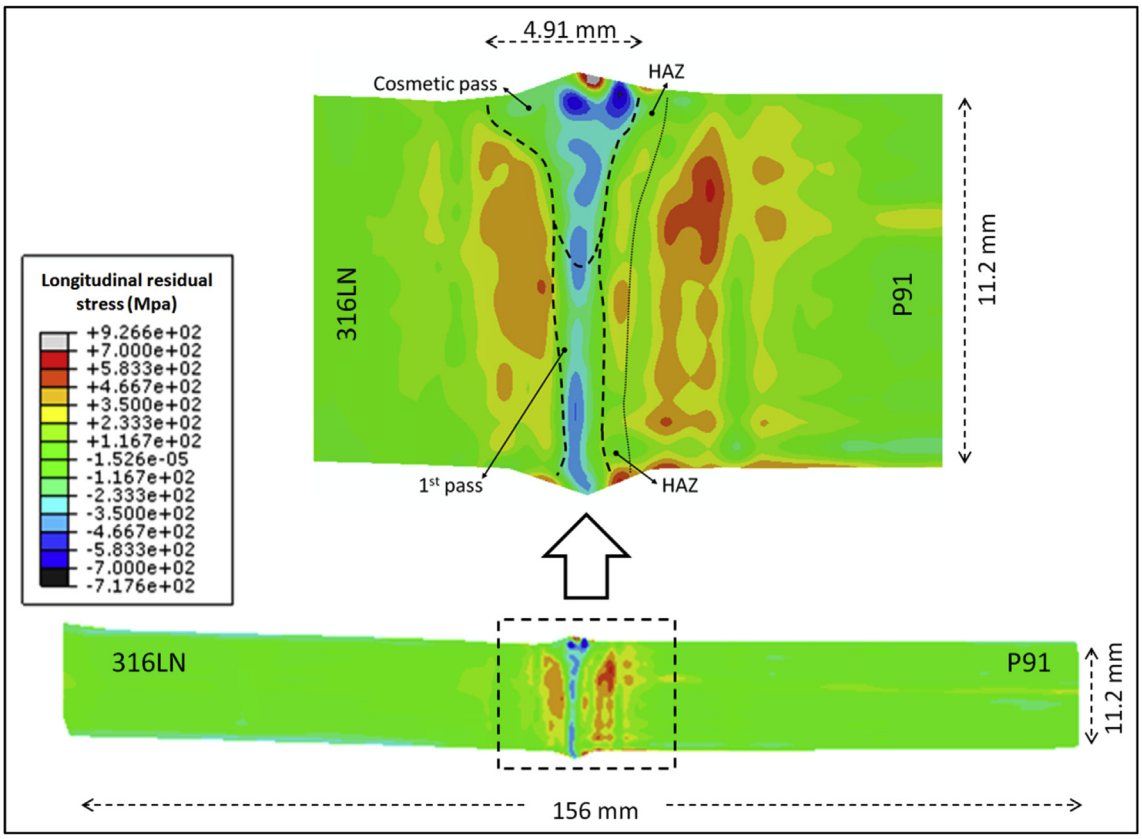

Fig. 7. RS measurement results achieved by the contour method (units in MPa).

3.1.2. Results achieved by neutron diffraction

The longitudinal residual stresses measured using neutron diffraction are shown in Fig. 9. Outside the central weld region, the stresses rise from very low values remote from the weld to ~400 MPa in parent material adjacent to the HAZ, in good qualitative agreement with the contour method measurements. The situation within the weld is more complex, since the sign of the measured stresses seems to depend upon the assumptions made about the phases present. Thus, compressive stresses are indicated on the P91 side of the weld region while tensile stresses are indicated on the AISI 316L(N) side. In addition to this divergence measured at the weld centreline, there are at least three points (at 0, -0.5 and −1 mm distance from the weld centerline) indicating an obvious measurement error as the RS reaches 900 MPa which is much higher than the yield strength of AISI 316L(N). The measurement of the lattice constants and subsequent strain calculations showed the presence of both tensile and compressive strains at the weld centreline. Abburi Venkata et al. [1] suggested that the diffraction pattern in the weld fusion zone contained reflections from both FCC and BCC phases, indicating a local segregation of these two phases in the fusion zone. However, it should be noted that there is a microstructural variation between the sample measurement location and the reference specimen. The stress free lattice parameter measurements were located inside the cosmetic pass; see Fig. 4b, while the longitudinal RS distribution, shown in Fig. 9, is inside the penetration pass. Furthermore, due to practical difficulties, stress free specimens were extracted from one end of welded plate while the strains were measured at a different location, at the centre of the weld length as shown in Fig. 4. A recent electron back scattering diffraction (EBSD) analysis of the weld fusion zone by Abburi Venkata et al. [43] showed that segregation of FCC and BCC phases in the cosmetic pass region is consistent with the observations from neutron diffraction results. When the gauge volume is properly filled, the peak position is fitted using a gauss fit to the data, with the mean at the centre of the gauge volume. However, in this project, the effect of partial gauge volume filling is because of the presence of both austenitic and ferritic phase at the interface of the HAZ and fusion zone in the 316L(N) side. Although the reflections are received from both the phases, the data is fit to reflections from only 316L(N). This partial filling of the gauge volume will generate an observable shift in the peak position which is misinterpreted as the strain due to the complication of distinguishing the shift from the actual strains. The shift is termed as pseudo strain leading to a raise in the measured residual stresses. Hence, the relatively high magnitude of stress observed in the AISI 316L(N) HAZ may be attributed to the gauge volume being partially filled with both weld and parent material [43]. The uncertainty in the ND results within the weld and HAZ confirms the necessity of using multiple RS measurement methods in order to reduce uncertainty particularly in the sensitive cases like DMW specimen investigated in this study.

3.1.3. Results achieved by the deep hole drilling method-DHD & iDHD

Results from the single through-thickness DHD/iDHD measurement are shown in Fig. 10. The iDHD stresses are generally somewhat higher than the DHD stresses, except for a single point near the bottom surface. This observation is consistent with minor plasticity-induced errors in the conventional DHD measurement. The measured stresses are tensile throughout the depth of the plate with slightly higher stresses adjacent to the cosmetic pass. The magnitude of the stresses is consistent with those measured at

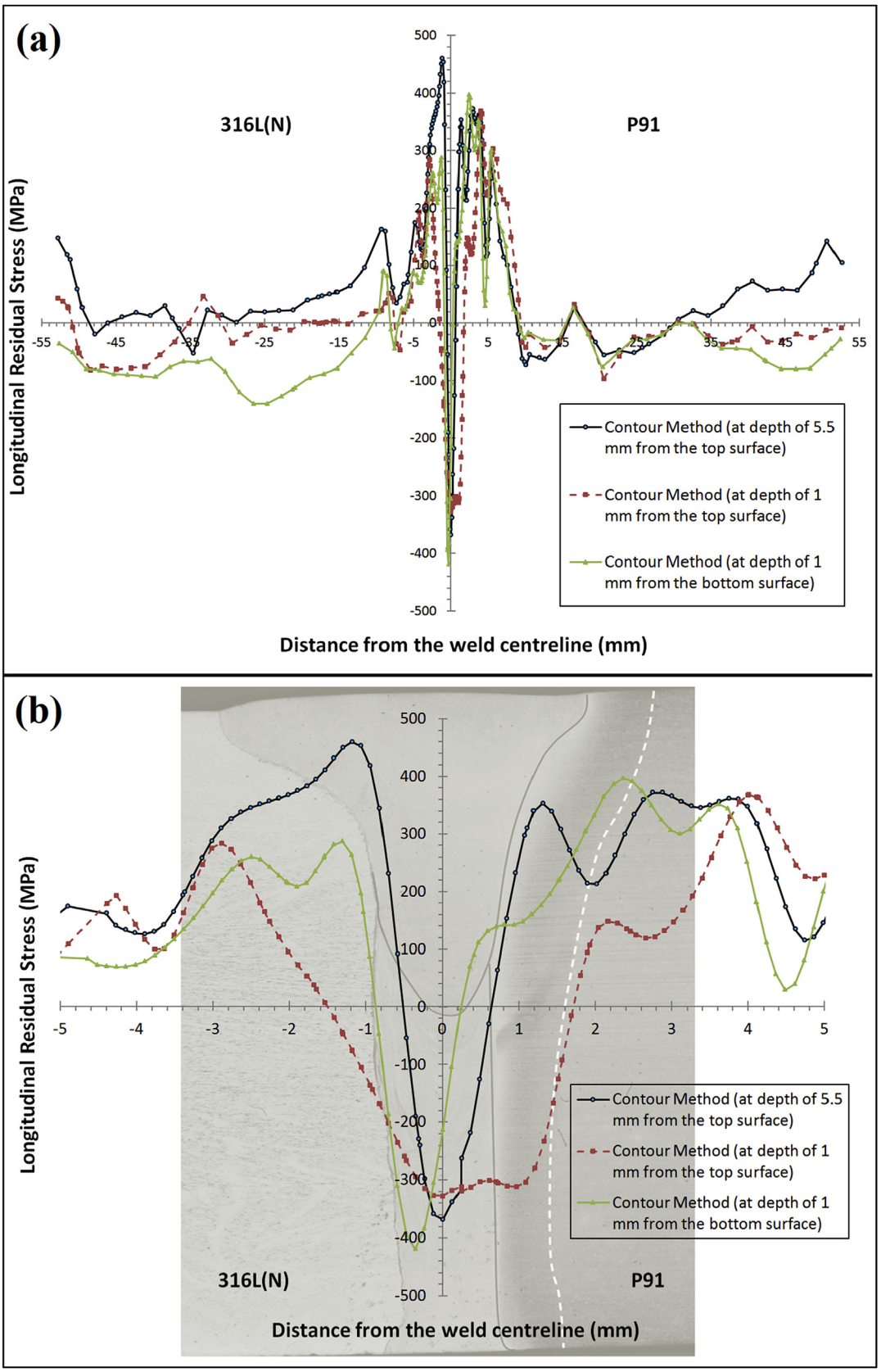

Fig. 8. The contour method result at a depth of 1 mm and 5.5 mm from the top surface as well as at 1 mm from the bottom surface, a) full width and b) the central 10 mm across the fusion boundary.

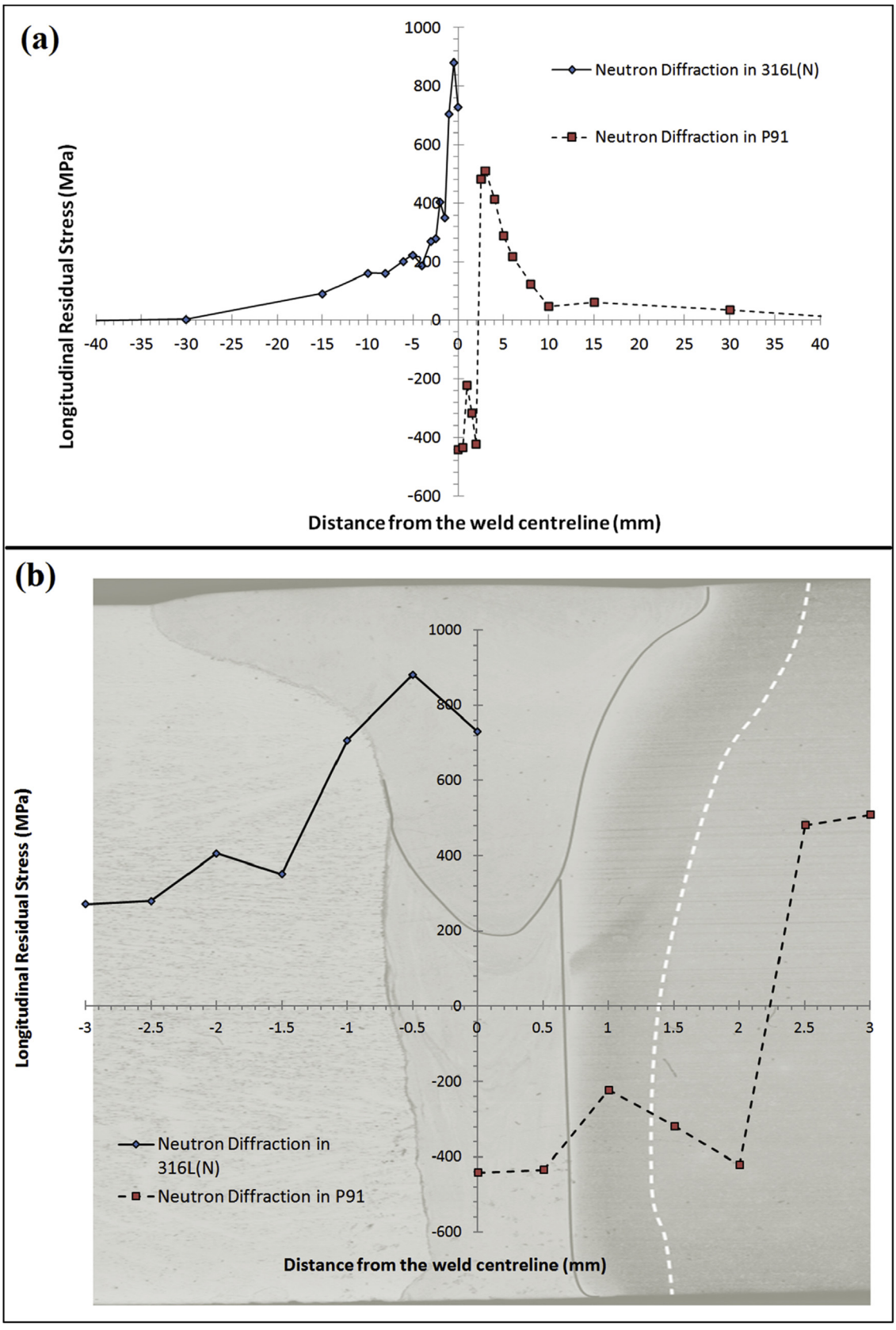

Fig. 9. RS measurement results achieved by the ND at 5.5 mm depth of the DMW specimen (a: whole the measurement line; b: weld and HAZ) [1].

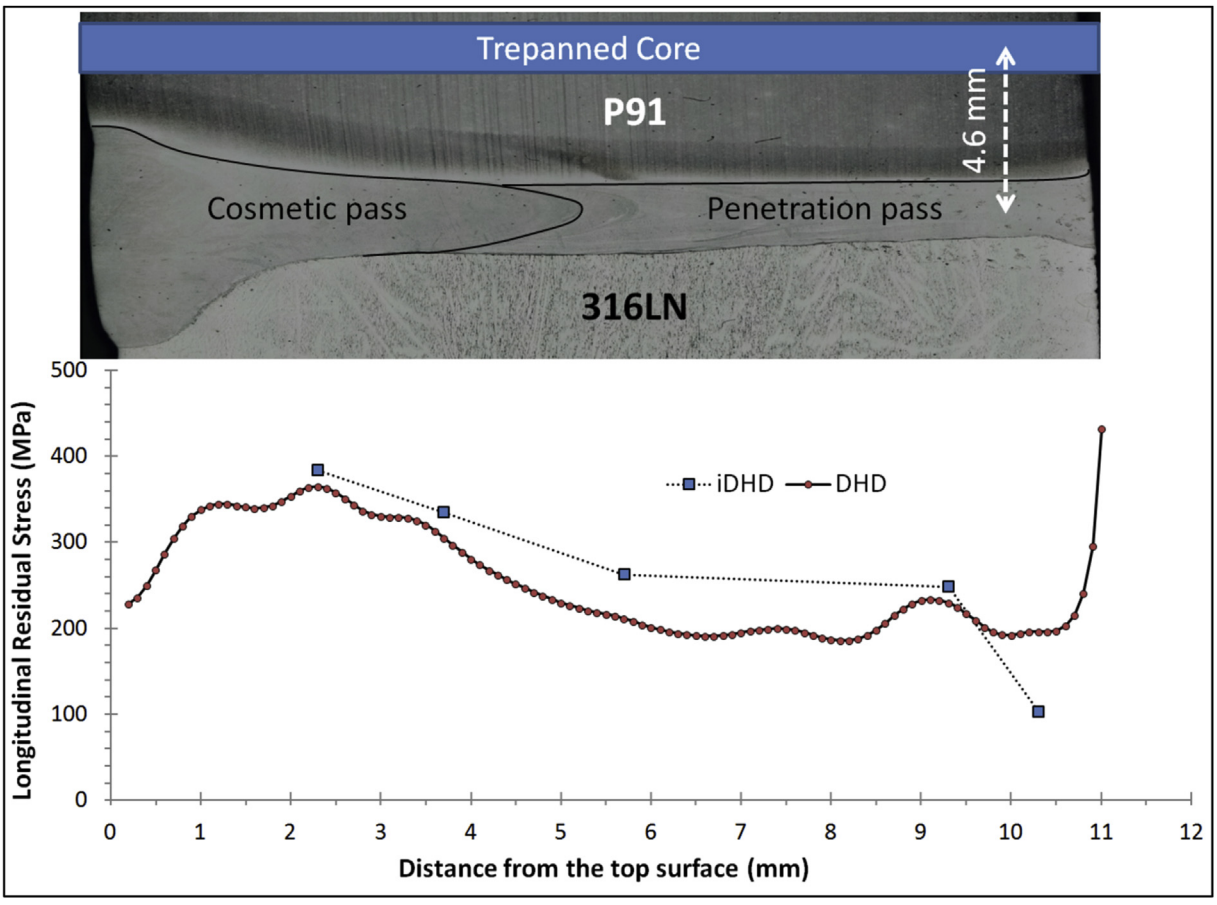

Fig. 10. RS measurement results achieved by the DHD and iDHD.

half-depth by neutron diffraction in P91 at a similar distance from the weld centreline. Near the bottom surface, the DHD and iDHD measurements diverge. It is normal to discard DHD data within 0.5–1 mm of the bottom surface of the plate, since they are affected by the proximity of the free surface. The plate is 11.2 mm thick, so on this basis, data at depths greater than 10.2 mm could be considered unreliable. Censoring on this basis will eliminate the divergence between DHD and iDHD techniques.

3.2. Surface stress measurements

3.2.1. Results achieved by X-Ray diffraction

Longitudinal residual stresses on the top surface of the specimen obtained from the XRD measurement are plotted in Fig. 11. The measurements reveal relatively low stresses in the AISI 316L(N) material remote from the welds, in the range −100 to +100 MPa. Close to the weld on the AISI 316L(N) side, the measured stresses rise to a peak of about 450 MPa about 5 mm from the weld centreline. Stresses in the weld bead (here the cosmetic pass) appear to be strongly compressive, at around −280 MPa (this value is obtained assuming that the weld bead behaves like P91 material). Measured stresses in P91 are very variable, ranging from about 100 MPa tension 5 mm from the weld to −300 MPa 15–25 mm from the weld.

Near-surface stresses measured using X-Ray diffraction are sensitive to the surface state and manufacturing history of the material, and may not be reflective of the bulk residual stress field developed during welding.

3.2.2. Results achieved by the shallow hole drilling method-iCHD

Incremental centre hole drilling (iCHD) was carried out at 8 points as shown in Fig. 12a. The measurement results shown in Fig. 12b represent the longitudinal residual stress measured at increments of 0.05 mm from the top surface up to a depth of 1 mm.

There are plenty of uncertainties (e.g., surface condition, material properties, gage position, hole misalignment, drilling parameters, drilling temperature, strain instrumentation output noise, data handling and skill of the operator) contributing to the reliability of the hole-drilling measurement [44]. For stresses that vary with depth, the overall effects of strain and depth uncertainties cannot be determined directly and another approach is required to establish reasonable uncertainty estimates for the computed stress values [44]. Shajer et al. [44] studied an example stress distribution to show uncertainty over the full depth range for a hole drilled in a steel specimen with hole depth increments varying from 32 μm at the surface to 128 μm at the full hole depth. The uncertainty analysis results showed a maximum value of ±40 MPa near to the surface (to a depth of around 200 μm) because of the relatively large effect of input uncertainties on the low levels of strains measured in the small hole depth increments. However, they reported lower uncertainties, reducing to a minimum of ±12 MPa around the mid-depth, and another increase to ±24 MPa at the full depth because of reducing sensitivity [44]. Although these uncertainties are dependent on the Young's modulus and Poisson's ratio of the specimen, from Fig. 12 it is believed that a somewhat similar approach can be observed in the DMW specimen as well. To this end, the results measured in depth range of 250 μm–800 μm are deemed to be most reliable and are therefore averaged and

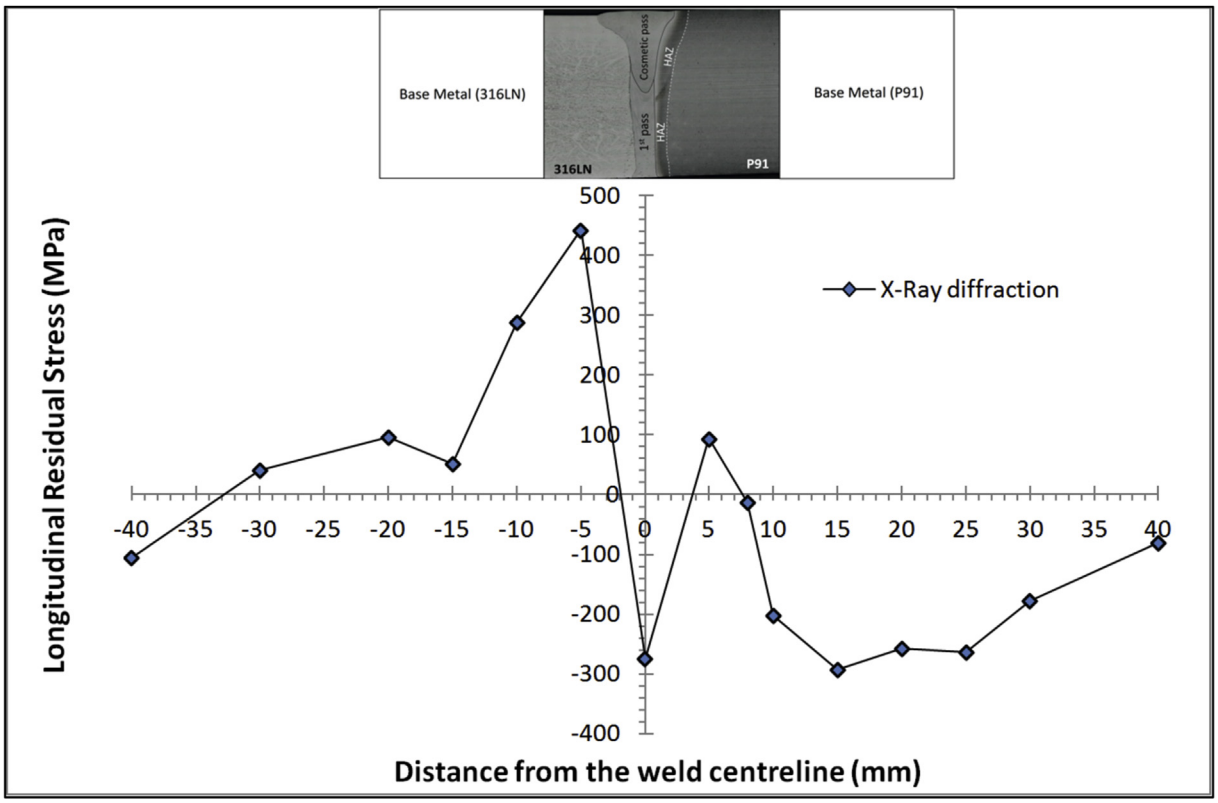

Fig. 11. RS measurement results achieved by the XRD.

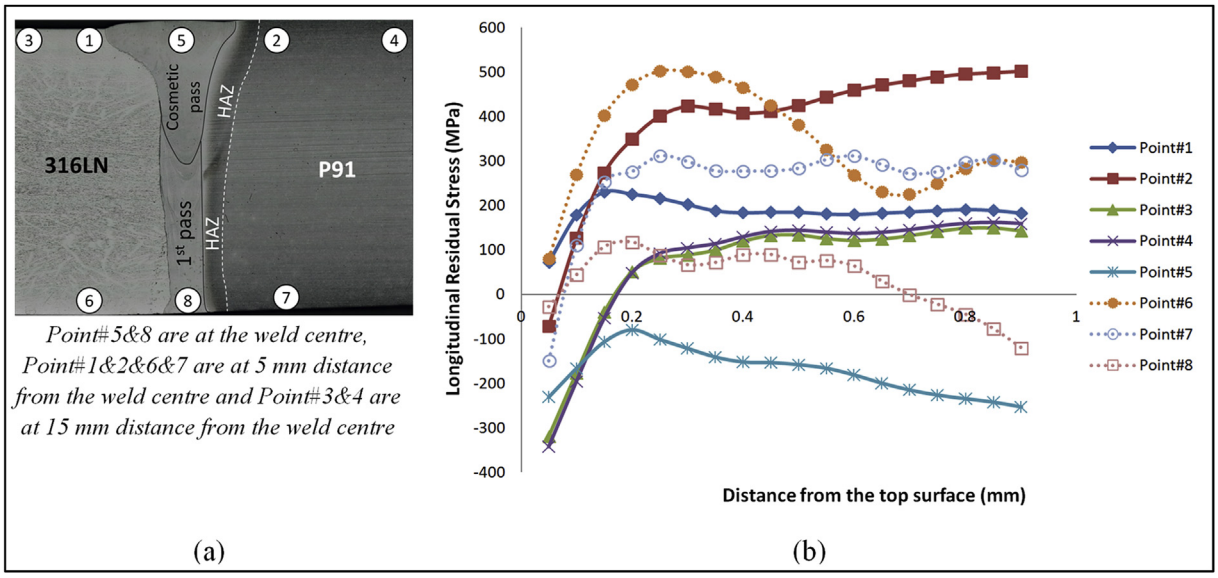

Fig. 12. Position of the points (a) and RS measurement results achieved by the iCHD (b).

tabulated in Table 4. The other results are believed to be measured with high uncertainty.

From Table 4, the top surface measurement shows compressive stress at the weld centre (−171 MPa) but tensile stress near the heat affected zone (HAZ) and inside the base metal on both sides of the weld. It is worth mentioning that the top surface measurement of the weld region is located inside the cosmetic pass as the iCHD depth is less than 1 mm. On the other side, the bottom surface measurement of the weld region is carried out inside the penetration pass showing tensile stress at the weld centre (49 MPa). Apart from the weld region, the magnitudes of the residual stresses in P91 are higher than those achieved in the AISI 316L(N) for the top surface measurement. Conversely, the bottom surface measurement showed higher RS in the AISI 316L(N) in comparison with that measured in the P91. This difference can be explained when looking at the point locations, Fig. 12a, showing that the Point#2 is very

Table 4
Average of the longitudinal residual stress measured by the iCHD at depth range of 250–800 μm.

Point number	Top surface			Point number	Bottom surface		
	Distance from the weld centre	Material	Average of the longitudinal RS		Distance from the weld centre	Material	Average of the longitudinal RS
Point#3	−15 mm	316L(N)	121 MPa	Point#6	−5 mm	316L(N)	362 MPa
Point#1	−5 mm	316L(N)	189 MPa				
Point#5	0	Weld (cosmetic pass)	−171 MPa	Point#8	0	Weld (penetration pass)	49 MPa
Point#2	5 mm	P91	444 MPa	Point#7	5 mm	P91	290 MPa
Point#4	15 mm	P91	133 MPa				

close to the HAZ of the P91 while Point#7 is not influenced by the HAZ. This proves a high magnitude of the residual stresses has been formed in HAZ region of the P91.

3.3. Round robin on the WRS measurement results

3.3.1. Measurement positions

The results achieved from all the stress measurement methods are compared in the bulk, mid-thickness of the plate, and on the surface, top and bottom surfaces. The top-surface measurements are inside the cosmetic pass while the mid-thickness and bottom-surface measurements are located in the penetration pass as listed in Table 5. All of the techniques have different gauge volume (see Table 5) and hence, the discrepancies between the results are expected due to the difference in gauge volume and measurement positions.

3.3.2. Bulk measurements

The longitudinal residual stresses measured at the mid-thickness located inside the penetration pass of the DMW specimen are re-plotted in Fig. 13. The measurement methods include:

I. The contour method (CM) at 5.5 mm depth.
II. The neutron diffraction (ND) method at 5.5 mm depth and by assuming P91 and AISI 316L(N) material properties separately.
III. The DHD at 5.5 mm depth (one point).
IV. The iDHD at 5.7 mm depth (no increment at 5.5 mm).

There is a good qualitative agreement between the three techniques, all of which are consistent with high tensile stresses in parent/HAZ material either side of the weld, and compressive stresses within the weld bed itself. Fig. 13 also highlights a number of potential issues with individual measurement techniques:

- There is some evidence of a potential offset of about 1 mm between ND and contour method measurements, revealed by the different signs apparently measured in the P91 HAZ between 1 mm and 2 mm from the weld centreline.
- The contour method may have under-measured the peak tensile stresses in the HAZ/parent region either side of the weld, by over-smoothing the very short wavelength stress distribution in this region.
- There is high uncertainty in the neutron diffraction measurements within and close to the weld fusion boundary: exemplified by the unrealistically high stresses measured in AISI 316L(N) adjacent to the fusion boundary, and in stresses in weld metal

Table 5
Round robin stress measurement positions.

	Measurement method	Measurement depth	Measurement gauge volume/diameter size	Measurement position			
				316L(N)	Weld	HAZ	P91
Bulk measurements (penetration pass)	Contour method	5.5 mm	EDM wire cut diameter: 50 μm CMM probe diameter: 1 mm CMM measurement pitch: 0.125 mm Optimised knot spacing: 0.5 mm FE mesh element size: 0.25 mm × 0.25 mm	×	×	×	×
	Neutron diffraction	5.5 mm	Gauge volume: 1 × 1 × 1 mm	×	×	×	×
	DHD	5.5 mm	Gun-drilled hole diameter: 1.5 mm Trepanned core external diameter: 4 mm				×
	iDHD	5.7 mm	Gun-drilled hole diameter: 1.5 mm Trepanned core external diameter: 4 mm				×
Top surface measurements (cosmetic pass)	Contour method	1 mm	EDM wire cut diameter: 50 μm CMM probe diameter: 1 mm CMM measurement pitch: 0.125 mm Optimised knot spacing: 0.5 mm FE mesh element size: 0.25 mm × 0.25 mm	×	×	×	×
	XRD	<30 μm	Irradiated area: 2 × 4 mm	×	×		×
	iCHD	0.25–0.8 mm (average)	Drilled hole diameter: 2 mm	×	×		×
	Neutron diffraction	1.5 mm	Gauge volume: 1 × 1 × 1 mm		×		
Bottom surface measurements (penetration pass)	Contour method	1 mm	EDM wire cut diameter: 50 μm CMM probe diameter: 1 mm CMM measurement pitch: 0.125 mm Optimised knot spacing: 0.5 mm FE mesh element size: 0.25 mm × 0.25 mm	×	×	×	×
	Neutron diffraction	2.2 mm	Gauge volume: 1 × 1 × 1 mm		×		
	iCHD	0.25–0.8 mm (average)	Drilled hole diameter: 2 mm	×	×		×

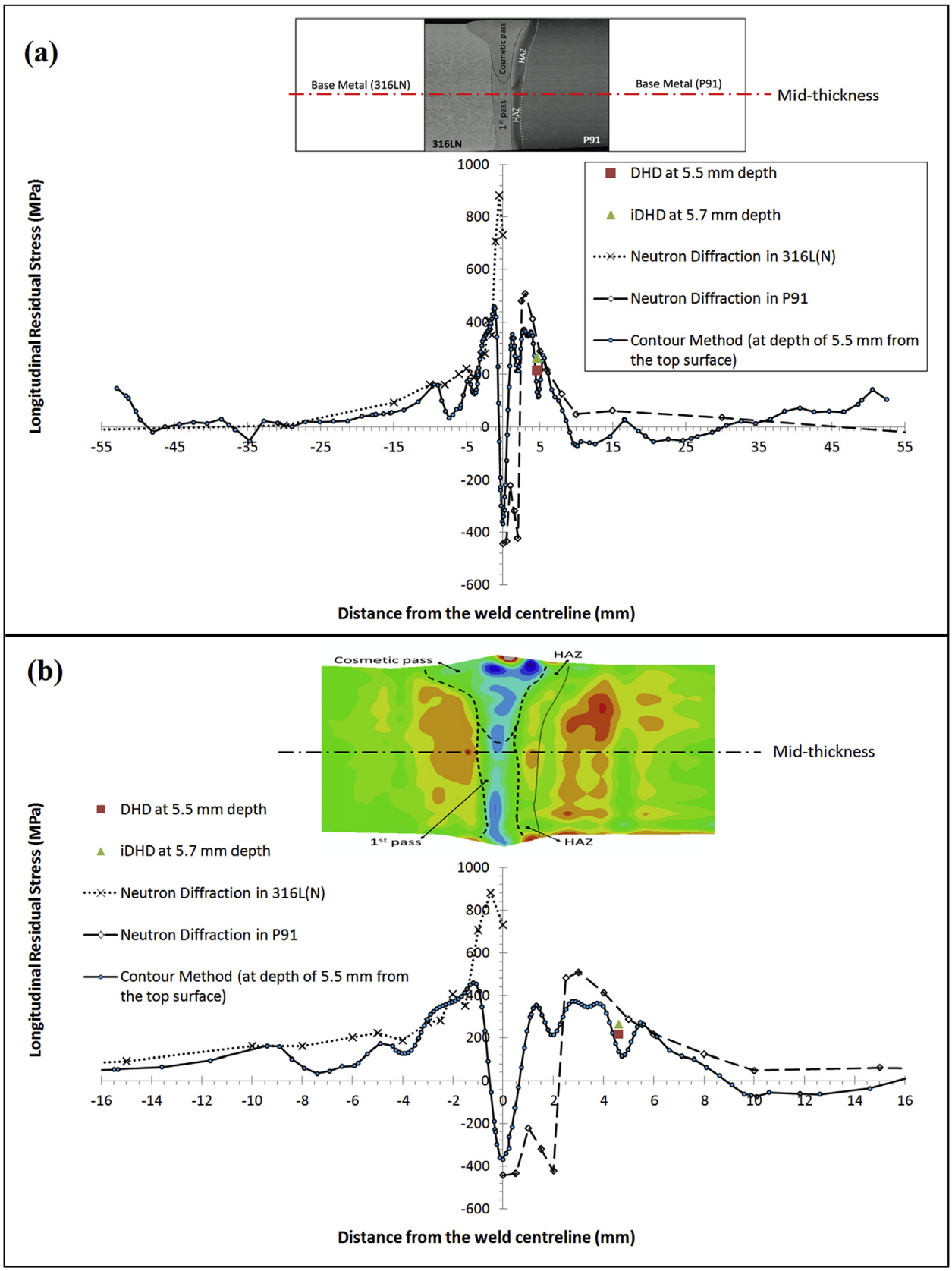

Fig. 13. Comparison between RS measurement methods at the mid-thickness, a) full width and b) the central 32 mm across the fusion boundary.

whose sign depends upon the assumptions made about the relevant stress-free lattice parameter.

The overall "M"-shaped residual stress distribution is consistent with the effects of low-temperature solid-state phase transformation (SSPT) on the stress state in high energy beam welds [41,42]. Thus the weld metal, which will have composition intermediate between AISI 316L(N) and P91, appears to have undergone a martensitic transformation at low temperature after solidification. The resulting volumetric expansion from FCC to BCC structure generates the compressive stresses observed in the weld bead. The change from tension to compression in the ND measurements at the weld centreline is not physically credible, being most probably an artefact of the handling of stress-free lattice parameters.

The sign of the stresses in the P91 HAZ has some uncertainty: the contour method measurements suggest stresses here are tensile, while the ND measurements suggest they are compressive. The ND stresses do however appear to have been offset, since they suggest compression outside the HAZ as well, which is not realistic. P91 has the capacity to generate reduced tensile or compressive stresses in regions of the HAZ that fully austenize during welding and then undergo low temperature SSPT on cooling. However, the P91 HAZ on the ND measurement line is in a region of the plate that will have undergone a second thermo-mechanical cycle during deposition of the cosmetic pass. If the cosmetic pass temperature transient does not result in austenisation, then tensile stresses are likely to develop during the cooling phase of the weld cycle (see Fig. 13b).

Peak tensile stresses occur in AISI 316L(N) close to the weld fusion boundary, and in P91 parent material outside the HAZ. If the unrealistic peak stresses reported close to the AISI 316L(N) fusion boundary are excluded, then the peak stresses on either side of the weld are approximately equal in magnitude, at 350–500 MPa.

3.3.3. Surface measurements

The following measured data are available for the top surface region:

A. The XRD method, which is an exclusively surface measurement method.
B. The iCHD method, from which the average results in the depth range 0.25–0.8 mm at Point#1 to Point#5 (see Table 4) are selected for the comparison.
C. A single point at 1.5 mm depth from a through-thickness line measurement made using neutron diffraction.
D. The contour method results at depth of 1 mm (see Fig. 8).

Care should be exercised in interpreting these data, since they relate to somewhat different depths, ranging from ~30 μm for XRD to 1.5 mm for neutron diffraction. The XRD measurements may be affected by localised stresses, such as those developed by machining, which the "bulk" techniques may not pick up. In addition, the contour method has higher uncertainty close to the edges of the measured specimen.

Fig. 14 shows a broad consensus on the AISI 316L(N) side of the weld with relatively low stresses remote from the weld rising to the tension of 200–400 MPa close to the fusion boundary. All four techniques record compressive stresses in the weld bead. The techniques then diverge on the P91 side of the weld. The differences are greatest in P91 parent material, where the XRD measurements indicate compressive stresses, while the other techniques suggest little stress (contour) or tension (ICHD). Given their different sampling depths, the most likely explanation is that the XRD measurements reveal localised machining or other forming stresses very close to the surface in parent material that, unlike the HAZ, has not undergone thermo-mechanical plasticity during welding, which would tend to remove them.

The longitudinal residual stresses at the bottom surface located inside the penetration pass of the DMW specimen are plotted in Fig. 15. The methods involved in this measurement are listed as follow:

i) The iCHD average results in Point#6, Point#7 and Point#8.
ii) The ND result at 2.2 mm depth.
iii) The CM results at depth of 1 mm (see Fig. 8).

The results measured by ND and CM show that the stresses are compressive at the weld centreline. Although the CM and iCHD results are consistent at 5 mm distance from the weld centreline, they diverge at −5 mm where the CM has encountered artefacts as mentioned before. This artefact is probably the reason for a deviation of around 270 MPa between iCHD and CM at −5 mm distance from the weld centreline.

4. Conclusions

In this study, five independent experimental methods were employed to measure the residual stresses in a DMW specimen manufactured by autogenous electron beam welding of a P91 ferritic-martensitic plate to an AISI 316L(N) austenitic stainless steel plate. These were neutron diffraction, x-ray diffraction, incremental centre hole drilling, deep hole drilling, and the contour method. Based on the achieved results, it can be concluded that:

1) The overall stress distribution is M-shaped, with tensile stresses of approximately 400 MPa in parent material on both sides of the weld, and compressive stresses of similar magnitude in the weld bead. These are characteristic of high energy beam welds where the weld molten zone undergoes low temperature solid state phase transformation from FCC to BCC in the final stages of cooling.
2) The presence of a cosmetic pass acts to concentrate peak tensile and compressive stresses adjacent to and within that pass rather than the penetration pass.
3) Peak tensile stresses at the mid-thickness occur close to the fusion boundary on the AISI 316L(N) side, and just outside the HAZ on the P91 side. The peak stresses on both sides appear to be similar, in the range 370–460 MPa. A region of slightly higher peak stress is also visible on the contour method map on the P91 side at about ¼ thickness.
4) Bulk stresses measured using neutron diffraction, the contour method, and deep hole drilling achieve good levels of agreement except in the weld bead and HAZ, where the ND stresses can become unrealistic. This is most likely due to a combination of positional uncertainty and uncertainty about the correct stress-free lattice parameter.
5) There is less agreement between different measurement methods at the top and bottom surfaces. This is probably mostly due to the different depths at which near-surface measurements from the different techniques are made, ranging from a few tens of microns for x-ray diffraction to about 1.5 mm for neutron diffraction.
6) The four techniques employed show broad agreement on the AISI 316L(N) side and in the weld bead, with low stresses remote from the weld, rising tension just outside the fusion boundary, and compression in the weld bead itself.
7) The x-ray measurements made on P91 parent material reveal significant compressive stresses outside the HAZ. It is likely that these are near-surface (not bulk) machining or forming stresses.

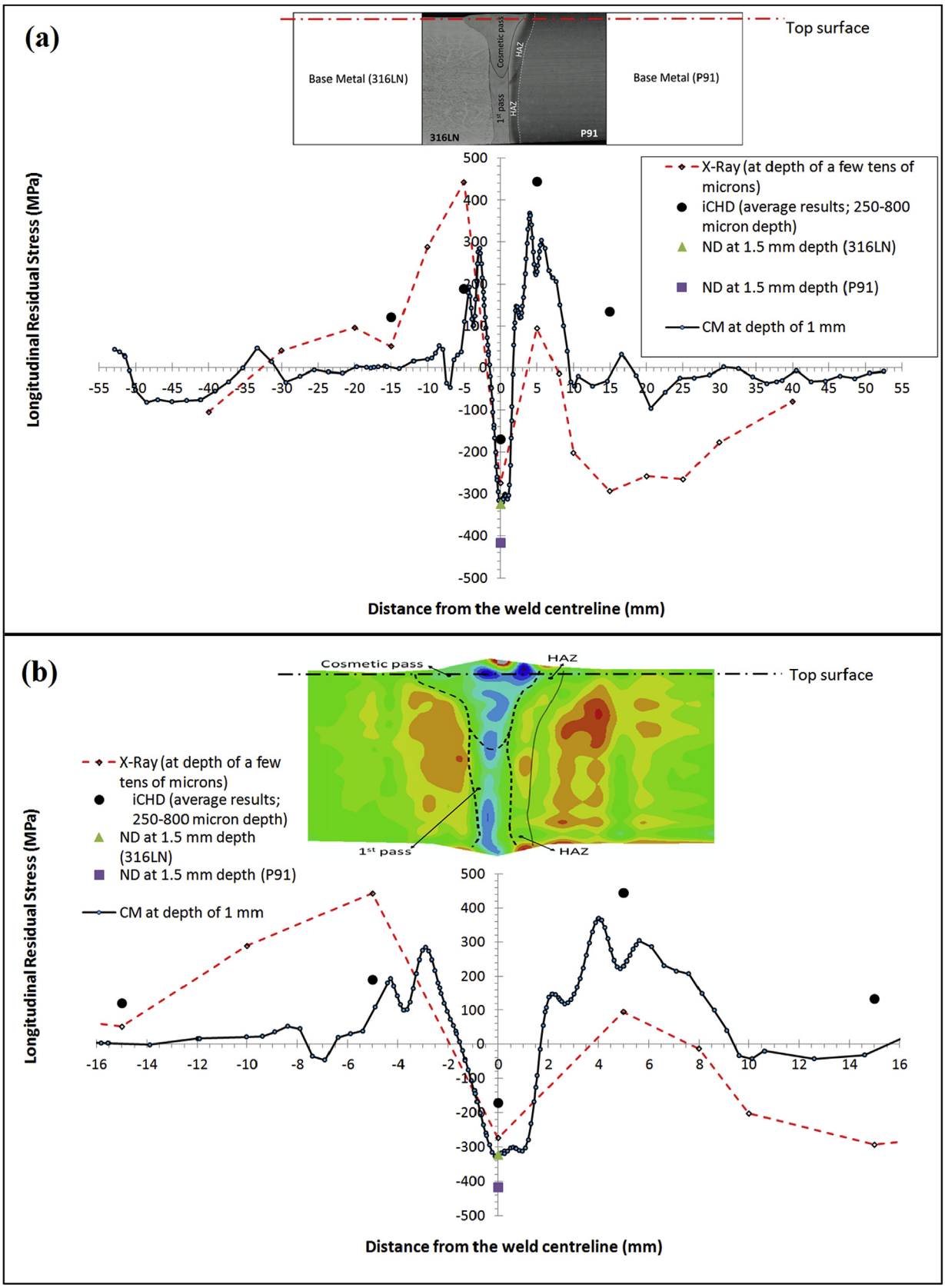

Fig. 14. Comparison between RS measurement methods at the top-surface, a) full width and b) the central 32 mm across the fusion boundary.

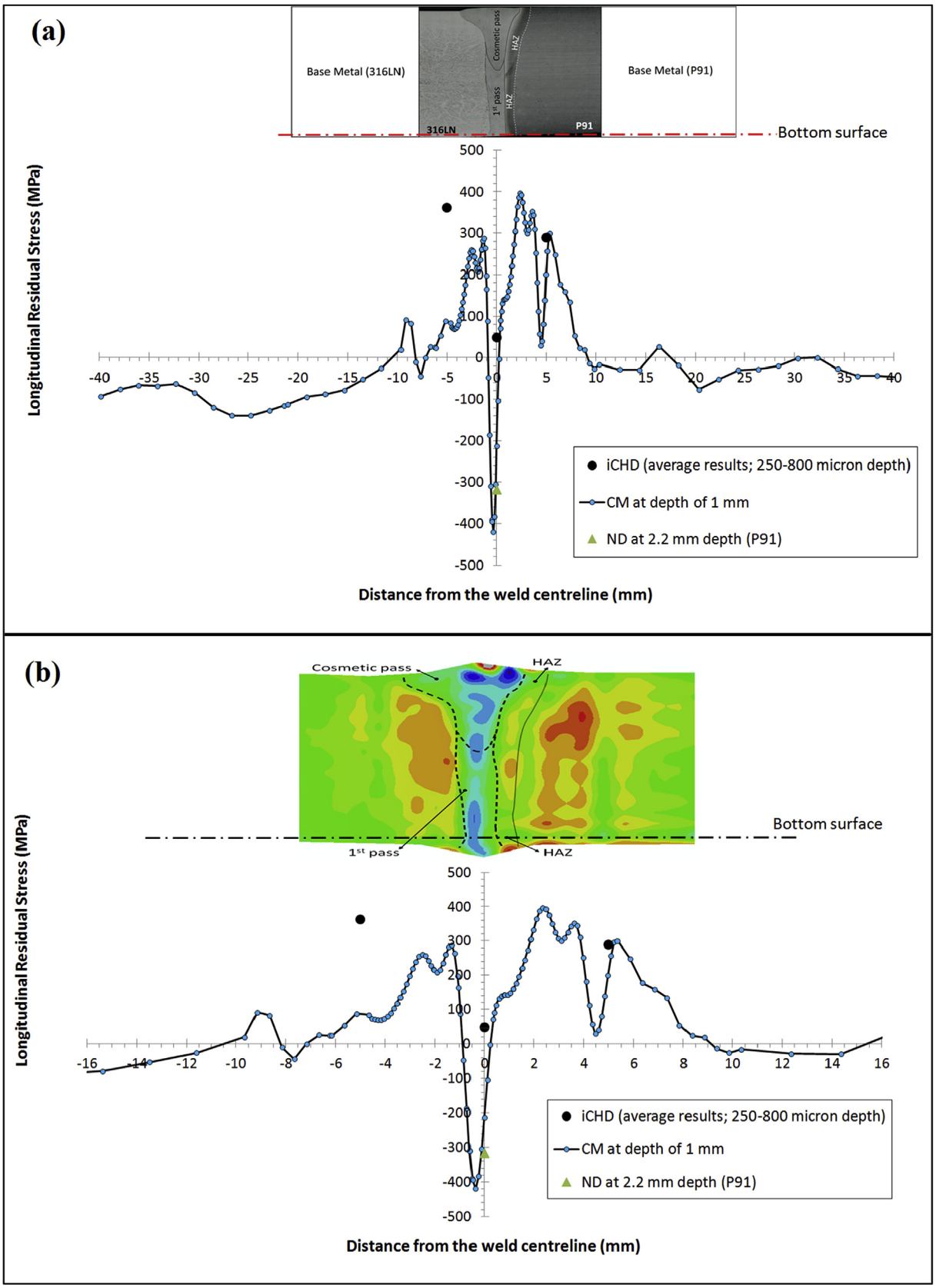

Fig. 15. Comparison between RS measurement methods at the bottom-surface, a) full width and b) the central 32 mm across the fusion boundary.

8) All five residual stress measurement techniques showed different uncertainties and potential errors. However, the deployment of so many independent techniques has allowed a reliable characterisation of the residual stresses in this challenging dissimilar metal weld.

Acknowledgements

This paper is a research output of an EPSRC project (EP/K007866/1) and is part of a national UK programme through the RCUK Energy programme and India's Department of Atomic Energy. The research involves the Universities of Bristol (UoB), Oxford and Manchester together with the Open University (OU). The authors then like to acknowledge EPSRC (EP/K007866/1) for the support and funding the project. Furthermore, valuable contributions of all staffs involved in hole drilling measurement and DHD at UoB, neutron diffraction measurement at Rutherford Appleton Lab, iCHD at VEQTER Ltd., XRD at IGCAR as well as contour method at OU are greatly appreciated.

References

[1] Venkata KA, Truman CE, Smith DJ, Bhaduri AK. Characterising electron beam welded dissimilar metal joints to study residual stress relaxation from specimen extraction. Int J Press Vessels Pip 2016;139:237–49.
[2] Chetal SC, Chellapandi P, Puthiyavinayagam P, Raghupathy S, Balasubramaniyan V, Selvaraj P, et al. Current status of Fast reactors and future plans in India. Asian Nucl Prospects 2010 2011;7:64–73.
[3] Javadi Y, Akhlaghi M, Najafabadi MA. Using finite element and ultrasonic method to evaluate welding longitudinal residual stress through the thickness in austenitic stainless steel plates. Mater Des 2013;45:628–42.
[4] Rossini NS, Dassisti M, Benyounis KY, Olabi AG. Methods of measuring residual stresses in components. Mater Des 2012;35:572–88.
[5] Fitzpatrick ME, Fry AT, Holdway P, Kandil FA, Shackleton JSL. A national measurement good practice guide, determination of residual stress by x-ray diffraction-issue 2. UK: National Physical Laboratory (NPL); 2005.
[6] Dai H, Francis JA, Stone HJ, Bhadeshia HKDH, Withers PJ. Characterizing phase transformations and their effects on ferritic weld residual stresses with x-rays and neutrons. Metall. Mater Trans a-Phy. Metall. Mater Sci 2008;39A:3070–8.
[7] Handbook of residual stress and deformation of steel. ASM Int; 2002.
[8] Prime MB, Hill MR, DeWald AT, Sebring RJ, Dave VR, Cola MJ. Residual stress mapping in welds using the contour method. Trends Weld Res Proc 2003: 891–6.
[9] Noyan IC, Huang TC, York BR. Residual-stress strain analysis in thin-films by x-ray-diffraction. Crit Rev Solid State Mater Sci 1995;20:125–77.
[10] Javadi Y, Pirzaman HS, Raeisi MH, Najafabadi MA. Ultrasonic stress evaluation through thickness of a stainless steel pressure vessel. Int J Press Vessels Pip 2014;123–124:111–20.
[11] Olabi AG, Hashmi MSJ. The effect of post-weld heat-treatment on mechanical-properties and residual-stresses mapping in welded structural steel. J Mater Process Technol 1995;55:117–22.
[12] Olabi AG, Casalino G, Benyounis KY, Rotondo A. Minimisation of the residual stress in the heat affected zone by means of numerical methods. Mater Des 2007;28:2295–302.
[13] Javadi Y. Investigation of clamping effect on the welding residual stress and deformation of monel plates by using the ultrasonic stress measurement and finite element method. J Press Vessel Technol.-Trans. Asme 2015;137.
[14] Javadi Y, Hasani M, Sadeghi S. Investigation of clamping effect on the welding sub-surface residual stress and deformation by using the ultrasonic stress measurement and finite element method. J Nondestruct Eval 2015;34.
[15] Javadi Y, Akhlaghi M, Najafabadi MA. Nondestructive evaluation of welding residual stresses in austenitic stainless steel plates. Res Nondestruct Eval 2014;25:30–43.
[16] Leggatt RH, Smith DJ, Smith SD, Faure F. Development and experimental validation of the deep hole method for residual stress measurement. J Strain Anal. Eng Des 1996;31:177–86.
[17] Traore Y, Bouchard PJ, Francis J, Hosseinzadeh F. A Novel cutting strategy for reducing plasticity induced errors in residual stress measurements made with the contour method. Pvp. 2011. In: Proceedings of the asme pressure vessels and piping conference, 6 a and B; 2012. p. 1201–12.
[18] EDF. Calculation of Residual Stress in Weldments, R6-Revision 4: chapter iii. Section III.15. EDF Energy Nuclear Generation Ltd.; 2014.
[19] Bouchard PJ. Code characterisation of weld residual stress levels and the problem of innate scatter. Int J Press Vessels Pip 2008;85:152–65.
[20] Kerr M, Prime MB, Swenson H, Buechler MA, Steinzig M, Clausen B, et al. Residual stress characterization in a dissimilar metal weld nuclear reactor piping system mock up. J Press Vessel Technol.-Trans. Asme 2013;135.
[21] Pagliaro P, Prime MB, Clausen B, Lovato ML, Zuccarello B. Known residual stress specimens using opposed indentation. J Eng Mater Technol.-Trans. Asme 2009;131.
[22] Pagliaro P, Prime MB, Robinson JS, Clausen B, Swenson H, Steinzig M, et al. Measuring inaccessible residual stresses using multiple methods and superposition. Exp Mech 2011;51:1123–34.
[23] Evans A, Johnson G, King A, Withers PJ. Characterization of laser peening residual stresses in Al 7075 by synchrotron diffraction and the contour method. J Neutron Res 2007;15:147–54.
[24] Moat RJ, Pinkerton AJ, Li L, Withers PJ, Preuss M. Residual stresses in laser direct metal deposited Waspaloy. Mater Sci Eng a-Struct. Mater Prop Microstruct Process 2011;528:2288–98.
[25] Zhang Y, Ganguly S, Edwards L, Fitzpatrick ME. Cross-sectional mapping of residual stresses in a VPPA weld using the contour method. Acta Mater 2004;52:5225–32.
[26] Kartal ME, Lijedahl CDM, Gungor S, Edwards L, Fitzpatrick ME. Determination of the profile of the complete residual stress tensor in a VPPA weld using the multi-axial contour method. Acta Mater 2008;56:4417–28.
[27] Withers PJ, Turski M, Edwards L, Bouchard PJ, Buttle DJ. Recent advances in residual stress measurement. Int J Press Vessels Pip 2008;85:118–27.
[28] Hosseinzadeh F, Toparli MB, Bouchard PJ. Slitting and contour method residual stress measurements in an edge welded beam. J Press Vessel Technol.-Trans. Asme 2012;134.
[29] Yaghi AH, Hyde TH, Becker AA, Sun W, Hilson G, Simandjuntak S, et al. A comparison between measured and modeled residual stresses in a circumferentially butt-welded P91 steel pipe. J Press Vessel Technol.-Trans. Asme 2010;132.
[30] Shan X, Davies CM, Wangsdan T, O'Dowd NR, Nikbin KM. Thermo-mechanical modelling of a single-bead-on-plate weld using the finite element method. Int J Press Vessels Pip 2009;86:110–21.
[31] ISO, ISO/TS 21432. Non-destructive testing – standard test method for determining residual stresses by neutron diffraction. Switzerland: International Organization for Standardization (ISO); 2005. 2010.
[32] VEQTER. Residual stress measurement. UK: VEQTER Residual Stress Experts; 2016.
[33] Fitzpatrick ME, Lodini A. Analysis of residual stress using neutron and synchrotron radiation. London: Taylor & Francis; 2003.
[34] Holden TM, Hutchings MT, Withers PJ, Lorentzen T. Introduction to the characterisation of residual stress by neutron diffraction. CRC Press; 2005.
[35] ASTM. Standard test method for determining residual stresses by the hole-drilling StrainGage method. ASTM E837-13a. West Conshohocken, PA, United States: ASTM; 2013. p. 1–16.
[36] Mahmoudi AH, Hossain S, Truman CE, Smith DJ, Pavier MJ. A new procedure to measure near yield residual stresses using the deep hole drilling technique. Exp Mech 2009;49:595–604.
[37] Prime MB. Cross-sectional mapping of residual stresses by measuring the surface contour after a cut. J Eng Mater Technol.-Trans. Asme 2001;123: 162–8.
[38] Hosseinzadeh F, Kowal J, Bouchard PJ. Towards good practice guidelines for the contour method of residual stress measurement (August, pg 1, 2014). J Eng.-Joe 2015:1–16. http://dx.doi.org/10.1049/joe.2014.0134.
[39] Traore Y. Controlling plasticity in the contour method of residual stress measurement. UK: Open University; 2013.
[40] Naveed N. Improving the spatial resolution of the contour method. UK: The Open University; 2015.
[41] Vasileiou AN, Smith MC, Jeyaganesh B, Francis JA, Hamelin CJ. The impact of transformation plasticity on the Electron Beam welding of thick-section ferritic steel components. United Kingdom: SMiRT-23Manchester; 2015.
[42] Vasileiou AN, Smith MC, Gandy D, Ferhati A, Romac R, Paddea S. Residual stresses in thick-section electron beam welds in rpv steels. In: ASME 2016 pressure vessels and piping conference (PVP2016). Vancouver, British Columbia, Canada: ASME; 2016.
[43] Venkata K Abburi, Truman CE, Coules HE, Warren AD. Applying electron backscattering diffraction to macroscopic residual stress characterisation in a dissimilar weld. J Mater Process Technol March 2017;241:54–63.
[44] Schajer GS, Whitehead PS. Hole drilling and ring coring. In: Schajer GS, editor. Practical residual stress measurement methods. Oxford, England: Blackwell Science Publ; 2013.